CELL STRESS

Mitochondrial redox sensing by the kinase ATM maintains cellular antioxidant capacity

Yichong Zhang[1], Ji-Hoon Lee[2], Tanya T. Paull[2], Sarah Gehrke[3], Angelo D'Alessandro[3], Qianhui Dou[4], Vadim N. Gladyshev[4], Elizabeth A. Schroeder[1], Samantha K. Steyl[5], Brooke E. Christian[5]*, Gerald S. Shadel[6]*

Mitochondria are integral to cellular energy metabolism and ATP production and are involved in regulating many cellular processes. Mitochondria produce reactive oxygen species (ROS), which not only can damage cellular components but also participate in signal transduction. The kinase ATM, which is mutated in the neurodegenerative, autosomal recessive disease ataxia-telangiectasia (A-T), is a key player in the nuclear DNA damage response. However, ATM also performs a redox-sensing function mediated through formation of ROS-dependent disulfide-linked dimers. We found that mitochondria-derived hydrogen peroxide promoted ATM dimerization. In HeLa cells, ATM dimers were localized to the nucleus and inhibited by the redox regulatory protein thioredoxin 1 (TRX1), suggesting the existence of a ROS-mediated, stress-signaling relay from mitochondria to the nucleus. ATM dimer formation did not affect its association with chromatin in the absence or presence of nuclear DNA damage, consistent with the separation of its redox and DNA damage signaling functions. Comparative analysis of U2OS cells expressing either wild-type ATM or the redox sensing–deficient C2991L mutant revealed that one function of ATM redox sensing is to promote glucose flux through the pentose phosphate pathway (PPP) by increasing the abundance and activity of glucose-6-phosphate dehydrogenase (G6PD), thereby increasing cellular antioxidant capacity. The PPP produces the coenzyme NADPH needed for a robust antioxidant response, including the regeneration of TRX1, indicating the existence of a regulatory feedback loop involving ATM and TRX1. We propose that loss of the mitochondrial ROS-sensing function of ATM may cause cellular ROS accumulation and oxidative stress in A-T.

INTRODUCTION

Ataxia-telangiectasia (A-T) is an autosomal recessive disease, pathology of which includes cerebellar neurodegeneration, cancer susceptibility, hypersensitivity to ionizing radiation, and immunodeficiency (*1*). A-T is caused by loss-of-function mutations in the gene encoding ATM (A-T mutated), a serine/threonine kinase belonging to the family of phosphatidylinositol 3-kinase–related kinases (*1*, *2*). ATM mediates nuclear DNA damage signaling and DNA double-strand break (DSB) repair and can promote cell cycle arrest and apoptosis (*1*, *2*). These activities are mediated by its phosphorylation of a large number of substrates, including the histone variant H2AX, the transcription factor p53, and checkpoint kinase 2 (CHK2) (*1*–*3*). When activated by DNA damage, ATM is converted from a noncovalent, inactive dimer into monomers that are recruited to DSBs by the MRE11/RAD50/NBS1 complex (*4*). In addition to defective nuclear DNA damage responses, A-T is also associated with oxidative stress that is thought to contribute to disease pathology (*1*, *5*, *6*). For example, higher levels of reactive oxygen species (ROS) contribute to increased lipid oxidation (*7*) and defects in neuronal cell proliferation (*8*, *9*), hematopoietic stem cell (HSC) exhaustion (*10*), and impaired B and T cell function (*11*, *12*). The cause of the oxidative stress in A-T remains uncertain but could be related to the redox-sensing function of ATM that was initially identified by Guo *et al.* (*13*) and is conserved in yeast (*14*). When activated by oxidative stress (such as in the presence of increased hydrogen peroxide), ATM forms disulfide-linked dimers that can phosphorylate some of its canonical substrates (such as CHK2) but signals in a manner distinct from the DNA damage response (*13*, *15*) and important for other downstream functions, including proteostasis (*16*). There are multiple disulfide linkages in the redox-sensing ATM dimer, and mutation of one of the cysteines involved to a leucine (C2991L) prevents redox signaling without affecting DNA damage signaling (*13*, *16*). Thus, analysis of this mutant provides the ability to dissect downstream consequences of the redox-sensing function of ATM (*16*), which we took advantage of in this study.

The pentose phosphate pathway (PPP) is an alternate route of glucose oxidation from glycolysis that generates nicotinamide adenine dinucleotide phosphate (NADPH) and ribose-5-phosphate. This pathway is essential for cellular redox homeostasis and DNA repair because NADPH is a reducing agent critical for maintaining the active, reduced forms of glutathione and thioredoxin needed for cellular antioxidant defenses and ribose-5-phosphate is a substrate for nucleotide biosynthesis needed for DNA repair (*17*). ATM is linked to the PPP through activation of the rate-limiting enzyme glucose-6-phosphate dehydrogenase (G6PD). This occurs by ATM-mediated phosphorylation of heat shock protein 27 (HSP27), which binds to and activates G6PD (*18*). Whether the redox-sensing function of ATM is related to its activation of cellular antioxidant defenses is an open question, but if so, this could

[1]Department of Genetics, Yale School of Medicine, New Haven, CT 06520, USA. [2]Howard Hughes Medical Institute, Department of Molecular Biosciences, University of Texas at Austin, Austin, TX 78712, USA. [3]Department of Biochemistry and Molecular Genetics, University of Colorado Denver, Aurora, CO 80045, USA. [4]Brigham and Women's Hospital, Harvard Medical School, Boston, MA 02155, USA. [5]Department of Chemistry, Appalachian State University, Boone, NC 28608, USA. [6]Salk Institute for Biological Studies, La Jolla, CA 92037, USA.
*Corresponding author. Email: gshadel@salk.edu (G.S.S.); christianbe@appstate.edu (B.E.C.)

represent a cellular antioxidant defense mechanism triggered by ROS signaling.

Multiple lines of evidence point to dysfunction of mitochondria as a component of A-T. As sites of the electron transport chain and other redox reactions (*19*), mitochondria are a major source of ROS and hence likely relevant to the oxidative stress in A-T. The initial observations of mitochondrial defects in A-T patient cells were aberrant mitochondrial morphology and respiration in lymphoblastoid cells (*20*) and mitochondrial DNA instability, downstream of defects in ribonucleotide reductase, in primary fibroblasts (*21*). Subsequently, A-T thymocytes were shown to have inefficient mitophagy, which in turn results in oxidative stress and adenosine 5′-triphosphate depletion due to accumulation of defective mitochondria (*22*). ATM also induces mitochondrial biogenesis through adenosine monophosphate–activated protein kinase in response to etoposide-induced DNA damage (*23*). Antioxidants have beneficial effects on cancer development and HSC defects in the *Atm*-null mouse models of A-T (*24*–*26*), and we previously showed that reducing mitochondrial hydrogen peroxide, by targeting the antioxidant enzyme catalase to mitochondria (mCAT), prolongs mean survival and partially rescues HSC and other immune system defects (*27*). Finally, we have also previously shown that reduced signaling through the nutrient-sensing mechanistic target of rapamycin complex 1 pathway leads to mitochondrial ROS–mediated changes in nuclear gene expression that are dependent on Tel1p and Rad53p, the yeast homologs of ATM and CHK2, but independently of their role in the nuclear DNA damage response (*14*). Activation of this pathway resulted in an adaptive response that led to increased stress resistance and longevity, which is fully recapitulated by transient exposure to low doses of the redox-cycling compound menadione that increases mitochondrial superoxide (*28*). This is one salient example of mitochondria as signaling organelles with ROS as the proximal messenger, which has been observed in many other physiological contexts (*29*, *30*). Here, we examined the potential role for mammalian ATM in mitochondrial ROS signaling and cellular antioxidant responses.

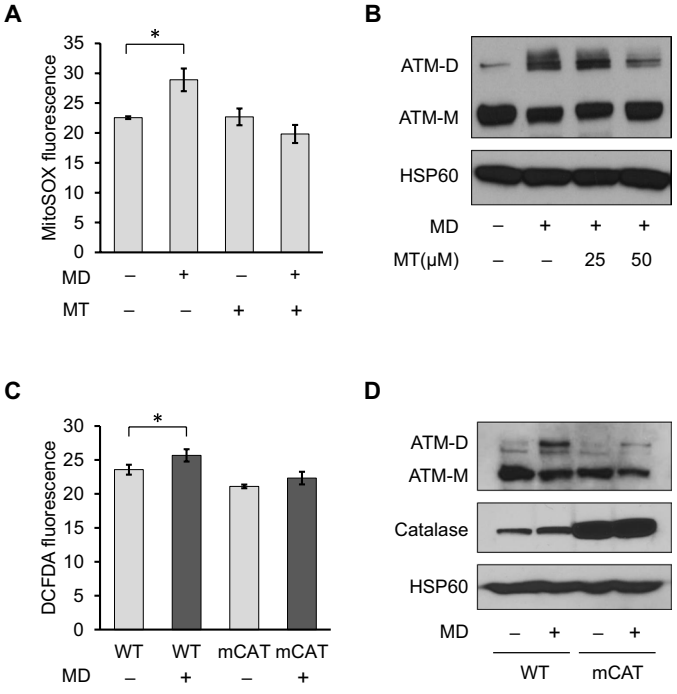

Fig. 1. Mitochondrial ROS promote redox-dependent ATM dimerization. (**A**) MitoSOX staining by flow cytometry in HeLa cells treated with vehicle (–) or 50 μM MitoTEMPO (MT; +) for 24 hours before being treated with vehicle (–) or 20 μM menadione (MD; +) for 30 min. Data are mean fluorescence intensities ± SD of biological triplicates. *$P < 0.05$ by Student's *t* test. (**B**) Western blot analysis of HeLa cells treated with vehicle (–) or 25 or 50 μM MitoTEMPO (+) for 2 hours before treatment with vehicle (–) or 20 μM MD (+) for 30 min. ATM monomers (ATM-M) and disulfide-linked dimers (ATM-D) were resolved by nonreducing SDS-PAGE. Mitochondrial HSP60 was probed as a loading control. (**C**) Primary MEFs from wild-type (WT) or mitochondrial catalase–overexpressing (mCAT) mice treated with vehicle or 20 μM MD for 30 min were analyzed for cellular ROS using 2′,7′-dichlorofluorescein diacetate (DCFDA) and flow cytometry as described in (A). (**D**) Western blots of ATM and HSP60 of MEFs treated as in (C) were performed as described in (B), except that catalase was also probed to demonstrate its overexpression. Blots are representative of three experiments.

RESULTS

ATM senses mitochondrial hydrogen peroxide

Using low doses of the redox-cycling chemical menadione to generate superoxide in mitochondria, we showed previously that the yeast homolog of ATM (Tel1p) is responsive to mitochondrial ROS and induces adaptive changes in nuclear gene expression that increase longevity (*14*, *28*). This response was separate from the role of Tel1p in nuclear DNA damage signaling. Mammalian ATM senses ROS by forming disulfide-linked dimers, but the cellular sources of ROS to which it is responsive have not been elucidated. Thus, to test for the involvement of mitochondrial ROS, we induced their production in HeLa cells using menadione. This resulted in increased mitochondrial ROS, as judged by MitoSOX staining (Fig. 1A), and promoted ATM dimer formation, which was probed in nonreducing, SDS–polyacrylamide gel electrophoresis (SDS-PAGE) gels (Fig. 1B, lane 2). Mitochondrial ROS and ATM dimer formation under these conditions were inhibited by the addition of the mitochondrial antioxidant MitoTEMPO (Fig. 1, A and B), consistent with mitochondrial ROS sensing. Menadione also induced cellular ROS and ATM dimer formation in primary mouse embryonic fibroblasts (MEFs), and this was inhibited in MEFs isolated from mCAT mice that have the hydrogen peroxide–scavenging enzyme catalase targeted to mitochondria (Fig. 1, C and D). These data indicate that the menadione-generated mitochondrial superoxide is converted to hydrogen peroxide that can exit mitochondria and promote ATM dimerization.

Inhibition of mitochondrial respiration can also lead to increased mitochondrial ROS production. However, treating HeLa cells with electron transport chain inhibitors, rotenone or antimycin A, at concentrations that increased mitochondrial superoxide to similar extent as menadione (Fig. 2A), did not result in ATM dimerization (Fig. 2C). Using MitoPY1, a fluorescent probe that senses mitochondrial hydrogen peroxide (*31*), we observed that menadione increased mitochondrial hydrogen peroxide, whereas rotenone and antimycin A did not (Fig. 2B). Peroxiredoxin 1 (PRDX1) is an antioxidant enzyme localized in the cytosol and nucleus that reacts with hydrogen peroxide (*32*, *33*). Similar to the MitoPY1 results, we found that PRDX1 was further oxidized to disulfide bond–linked dimers by menadione but not by rotenone or antimycin A (Fig. 2C). These results demonstrate that mitochondrial

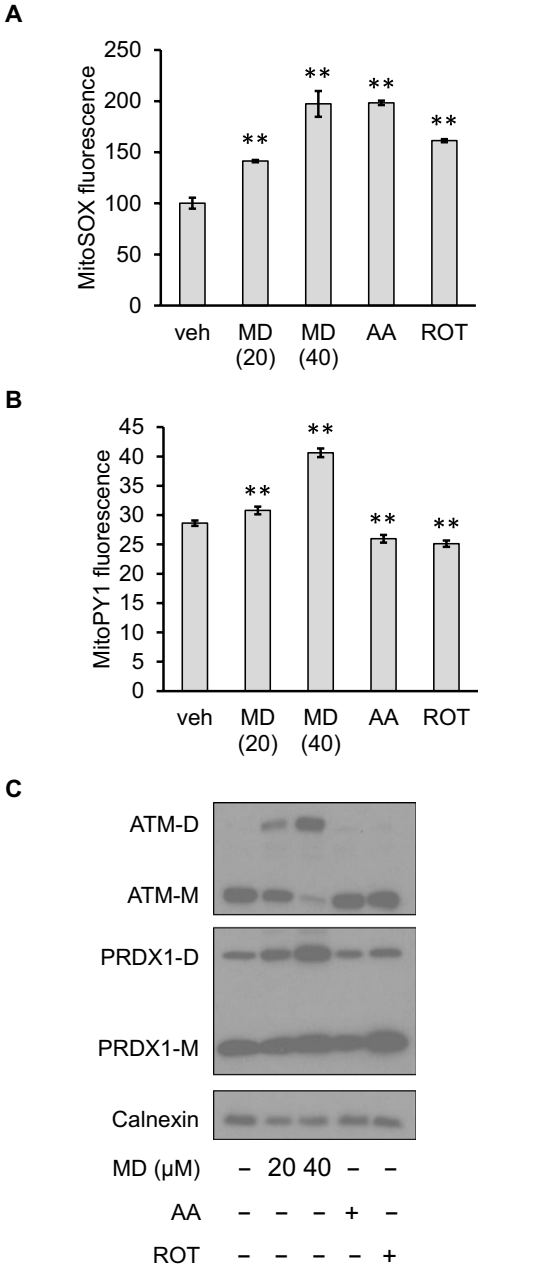

Fig. 2. Conversion of mitochondrial superoxide to membrane-permeable hydrogen peroxide is necessary for ATM dimerization. (**A**) MitoSOX staining in HeLa cells treated with vehicle (veh), 20 or 40 μM MD, 2 μM antimycin A (AA), or 0.4 μM rotenone (ROT) for 30 min. Data are mean fluorescence intensities ± SD of biological triplicates. $^{**}P < 0.01$ by Student's *t* test. (**B**) MitoPY1 staining in HeLa cells treated with vehicle, 20 or 40 μM MD, 2 μM antimycin A, or 0.4 μM rotenone for 30 min. Plotted is the mean fluorescence intensity ± SD of biological triplicates. $^{**}P < 0.01$ by Student's *t* test. (**C**) Western blot analysis of HeLa cells treated with vehicle (–), 20 or 40 μM MD, 2 μM antimycin A, or 0.4 μM rotenone for 30 min. ATM monomers and dimers and PRDX1 monomers (PRDX1-M) and dimers (PRDX1-D) were resolved by nonreducing SDS-PAGE. Calnexin was probed as a loading control. Blots are representative of three experiments.

superoxide must be converted to hydrogen peroxide to gain access to the cytosol and/or nucleus to dimerize ATM and other redox reactive proteins.

ATM redox dimers are localized to the nucleus but do not inhibit DNA damage signaling

Paull and colleagues have shown in several contexts that the redox and DNA damage sensing functions of ATM are distinct (*13*, *16*). Consistent with this, in HeLa cells, menadione increased ATM-dependent phosphorylation of CHK2 but not of γH2AX (Fig. 3A), indicating that ATM activation by mitochondrial ROS is not the result of nuclear DNA DSBs. Conversely, inducing nuclear DNA damage with topotecan, a topoisomerase I inhibitor, led to phosphorylation of CHK2 and H2AX but not dimerization of ATM (Fig. 3A). We next investigated the cellular localization of ATM and ATM dimers. In different cell types, ATM has been reported to localize to the nucleus, cytoplasm, mitochondria, and peroxisomes (*22*, *34*–*36*). In HeLa cells, we found that both ATM monomers and dimers resided primarily in the nucleus based on biochemical fractionation studies (Fig. 3B). Given that nuclear ATM is recruited to chromatin after DNA damage and we found ATM dimers in the nucleus, we hypothesized that ATM dimerization might interfere with its recruitment to chromatin. However, when we treated HeLa cells with menadione and topotecan to induce mitochondrial ROS and DNA damage simultaneously, we observed that ATM dimerization did not affect the ability of ATM to bind to chromatin basally or in the presence of DNA damage (Fig. 3C). This again indicates that redox signaling and DNA damage signaling by ATM are largely independent and that mitochondrial hydrogen peroxide signaling can promote ATM dimerization in the nucleus.

Thioredoxin 1 reduces ATM dimers

Thioredoxin 1 (TRX1) is a redox-responsive enzyme found in the nucleus and cytoplasm that reduces protein disulfide bonds (*37*). Because we found that ATM dimers are mostly located in the nucleus in HeLa cells and that their formation can be mediated by mitochondrial hydrogen peroxide, we explored whether TRX1 is involved in regulating this pathway. TRX1 knockdown in HeLa cells led to increased ATM dimerization basally (Fig. 4A) and greater dimer formation in response to low concentrations of menadione (Fig. 4A). In the absence of menadione, TRX1 knockdown had no effect on cellular ROS abundance but did exacerbate menadione-induced ROS production (Fig. 4B). To better characterize the effect of TRX1 on ATM dimers, we examined their stability in the presence and absence of TRX1 knockdown. To do this, we induced the formation of dimers with menadione, then changed the media to that without menadione, and monitored their rate of decay. In the presence of TRX1, ATM dimers exhibited a half-life of ~30 min, whereas TRX1 knockdown significantly increased the half-life of ATM dimers (Fig. 4C). In this experiment, menadione-induced ROS returned to baseline abundance within 30 min after the media change in both control and TRX1 knockdown cells (fig. S1A). In addition, oxidized PRDX1 and PRDX2 are reported to promote protein oxidation through redox relays (*38*, *39*), leading us to examine their potential role in ATM dimerization. Knocking down PRDX1 and PRDX2 by small interfering RNA (siRNA) (Fig. 4D) or knocking them out using clustered regularly interspaced short palindromic repeats (CRISPR) technology (fig. S1B) failed to prevent ATM dimerization induced by menadione, suggesting that PRDX1 and PRDX2 are not required.

ATM redox signaling activates the PPP through increased expression of G6PD

We next wondered why ATM might sense mitochondrial ROS and reasoned that it might be part of a cellular antioxidant response.

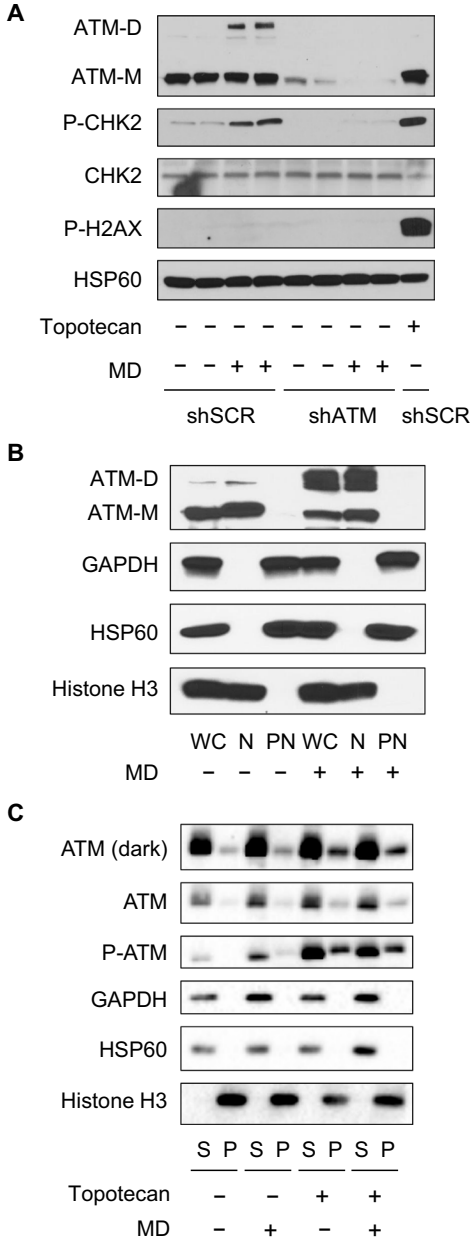

Fig. 3. Mitochondrial hydrogen peroxide–induced ATM dimers are in the nucleus but do not interfere with ATM chromatin association. (**A**) Western blot analysis of HeLa cells expressing short hairpin RNA (shRNA) targeting a scrambled sequence (shSCR) or ATM (shATM) treated with 20 μM MD (+) or vehicle (ethanol; –) for 30 min or 0.75 μM topotecan for 1 hour, as indicated. ATM dimer, ATM monomer, CHK2, phosphorylated CHK2 Thr^{68} (P-CHK2), and phosphorylated H2AX Ser^{139} (P-H2AX) were probed, along with HSP60 as a loading control. (**B**) HeLa cells treated with vehicle (ethanol; –) or 30 μM MD (+) for 1 hour were separated into nuclear (N) and postnuclear (PN) fractions, which were analyzed by Western blot along with a cell-equivalent amount of whole-cell (WC) lysate. ATM monomer, ATM dimer, histone H3, glyceraldehyde-3-phosphate dehydrogenase (GAPDH), and HSP60 were analyzed. (**C**) HeLa cells treated with vehicle (–) or 20 μM MD (+) for 30 min and/or 0.75 μM topotecan for 1 hour were subjected to salt extraction of chromatin-bound proteins. An equivalent volume of the supernatant fraction (S) and the pellet (P) fraction (containing chromatin-bound proteins) was loaded for Western blot. ATM, phosphorylated ATM Ser^{1981} (P-ATM), histone H3, GAPDH, and HSP60 were analyzed. Blots are representative of two experiments.

The PPP is an alternate route of glucose metabolism that generates NADPH needed to maintain cellular antioxidant responses and to supply ribose-5-phosphate for nucleotide synthesis and DNA repair (*17*). ATM is known to activate the PPP under DNA damage conditions through its phosphorylation of HSP27, a positive regulator of G6PD (*18*), the rate-limiting enzyme in the pathway. Thus, we hypothesized that the redox-sensing function of ATM might also be involved in regulating the PPP, perhaps by a similar mechanism. To test this, we used a U2OS cell system devised by Lee *et al.* (*16*) that enabled comparison of cells expressing either WT ATM or the C2991L mutant that is deficient in redox signaling (*13*). In this system, endogenous ATM is knocked down by shRNA and replaced by the WT or mutant protein (for further details, see Materials and Methods). In these cells, we observed robust knockdown of endogenous ATM and similar expression of WT and C2991L ATM protein expressed ectopically (fig. S2A). Under these conditions, relative to cells expressing the C2991L mutant, those expressing WT ATM had significantly lower DCFDA staining in the presence and absence of menadione (Fig. 5A) and maintained lower MitoSOX staining in the presence of menadione (Fig. 5B). These data indicate that ATM redox signaling is needed to maintain lower cellular and mitochondrial ROS abundance. We next asked whether this was due to lack of HSP27 phosphorylation; however, this was not the case (fig. S2B). Instead, we observed higher G6PD activity in cells expressing WT ATM compared to the C2991L mutant (Fig. 5C) that correlated with higher amounts of G6PD mRNA and protein (Fig. 5, D and E).

To further validate this new mode of PPP regulation by ATM, we performed metabolic tracing experiments with $^{13}C_{1,2,3}$-glucose in U2OS cells expressing WT or C2991L-mutant ATM. This approach can distinguish metabolic flux through either glycolysis or the PPP. Increased relative flux through the PPP is expected to generate more hexose and pentose phosphate intermediates and by-products of the PPP (Fig. 6A). At 6 and 24 hours after adding $^{13}C_{1,2,3}$-glucose, more light and heavy (M + 2) ribose phosphate (and pentose phosphate isobaric isomers) and a higher 6-phosphogluconate/glucose-6-phosphate ratio was observed in the U2OS cells expressing WT ATM compared to the C2991L mutant (Fig. 6, B and C), indicating more flux through the PPP in the WT cells.

Catabolism of $^{13}C_{1,2,3}$-glucose generates distinct isotopologues of lactate, either M + 2 and M + 3, depending on whether glucose oxidation preferentially occurs through the PPP or the glycolytic pathway (fig. S3A). We observed increased glucose consumption and lactate generation through glycolysis in the C2991L-mutant cells (fig. S3, B and C). These cells also exhibited increased shuttling of glucose-derived heavy carbons into the tricarboxylic acid (TCA) cycle (fig. S4). Last, our metabolic flux analysis revealed that C2991L cells produced more heavy glutathione than WT ATM cells (Fig. 6D), suggesting an increased rate of glutathione synthesis. This was confirmed by the higher steady-state levels of glutathione in the C2991L cells (fig. S5A). However, despite the higher total level of glutathione, there was no difference in the glutathione/glutathione disulfide (GSH/GSSG) ratio (fig. S5B). Together, these data demonstrate a role of ATM redox sensing in the shunting of glucose catabolism toward the PPP for redox and anabolic purposes, and that there is a disruption of glutathione homeostasis when this function of ATM is lost.

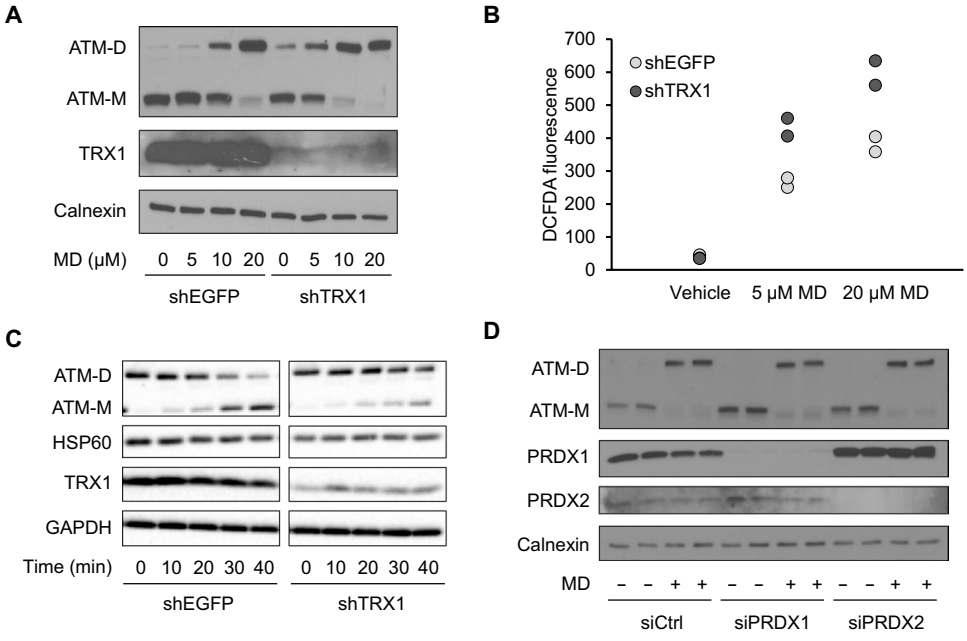

Fig. 4. TRX1 negatively regulates ATM redox dimerization. (**A**) Western blot analysis of HeLa cells expressing shRNA-targeting enhanced green fluorescent protein (shEGFP) as a negative control or TRX1 (shTRX1) treated with vehicle or the indicated concentration of MD for 30 min. Blot was probed for ATM monomer, ATM dimer, and TRX1, with calnexin as a loading control. Blots are representative of two experiments. (**B**) DCFDA staining by flow cytometry, in cells treated with vehicle, 5 or 20 μM MD as described in (A). Plot is representative of three experiments using biological duplicate samples in each. (**C**) Western blot of HeLa cell treated with 20 μM MD for 30 min after which the medium was changed and cells were allowed to recover for 0, 10, 20, 30, and 40 min, as indicated. Blot was probed for ATM monomer, ATM dimer, and TRX1, with HSP60 and GAPDH as loading controls. Blots are representative of three experiments. (**D**) Western blot of HeLa cells transfected with control (siCtrl) or siRNA-targeting PRDX1 and PRDX2 for 72 hours and treated with vehicle (–) or 20 μM MD (+) for 30 min. Blot was probed for ATM monomer, ATM dimer, PRDX1, and PRDX2, with calnexin as a loading control. Blots are representative of three experiments.

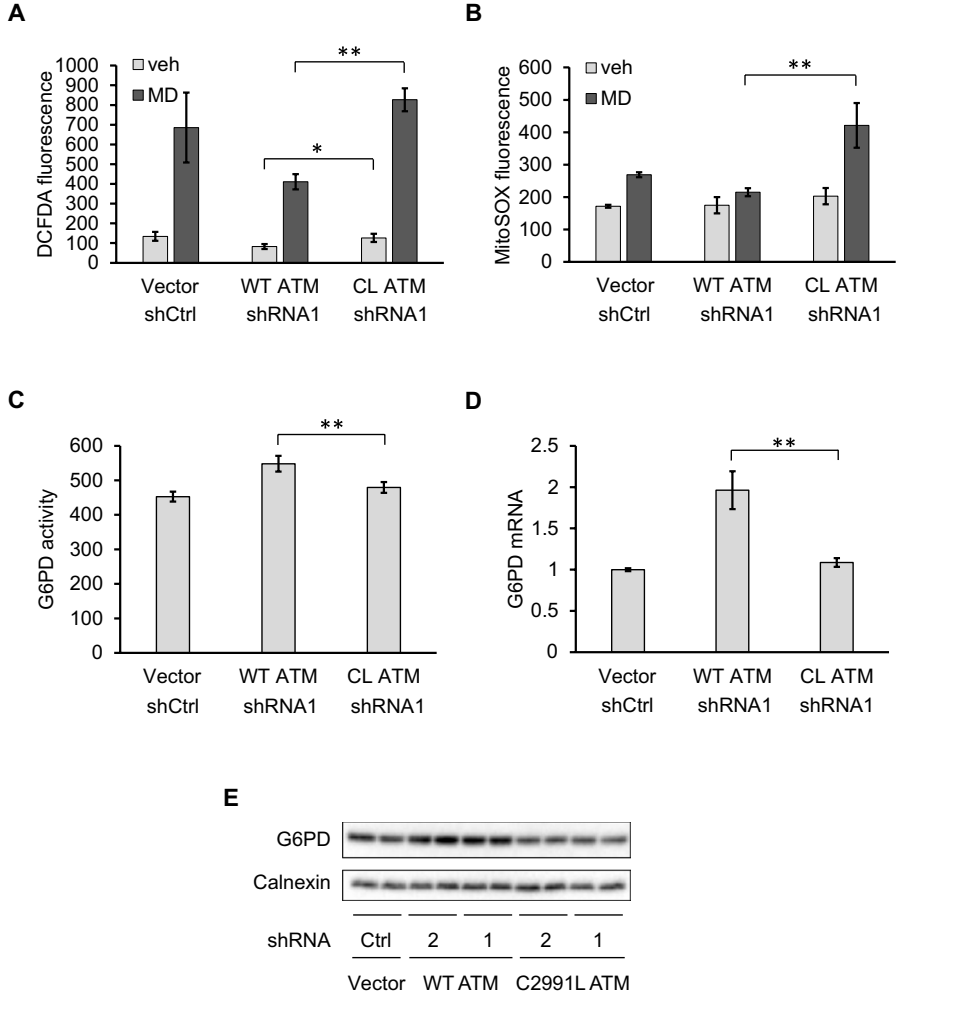

Fig. 5. Redox sensing by ATM up-regulates antioxidant capacity and G6PD expression. (**A** and **B**) Analysis of U2OS cells transfected with empty vector (vector) and control shRNA (shCtrl) or overexpressing WT or the C2991L (CL)–mutant ATM while having their endogenous ATM knocked down by shRNA-targeting ATM (shRNA1) were treated with vehicle or 20 μM MD for 30 min. Cellular and mitochondrial ROS were then measured by DCFDA (A) or MitoSOX (B) staining and flow cytometry. Plotted is the mean fluorescence intensity ± SD of biological triplicates. $^{*}P < 0.05$ and $^{**}P < 0.01$ by Student's *t* tests. (**C**) G6PD activity. Plotted is the mean ± SD of technical quadruplicates from a representative of three experiments. $^{**}P < 0.01$ by Student's *t* tests. (**D**) G6PD mRNA abundance by quantitative polymerase chain reaction (qPCR). Plotted is the mean ± SD of biological triplicates. $^{**}P < 0.01$ by Student's *t* tests. (**E**) Western blot of G6PD protein. Here, endogenous ATM was knocked down by one of two shRNAs (1 and 2). Calnexin was probed as a loading control. Blots are representative of three experiments.

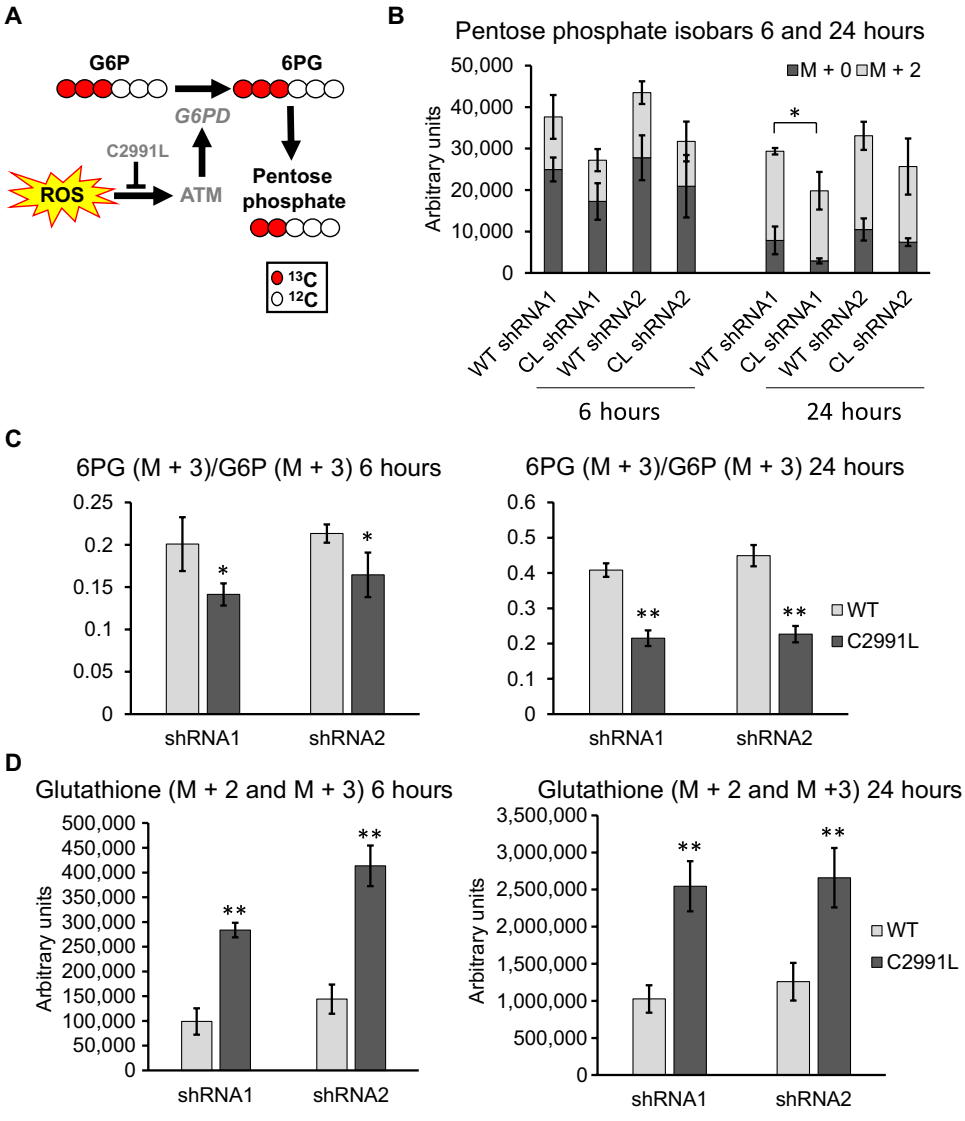

Fig. 6. Cells deficient in ATM redox signaling flux less glucose through the PPP and have increased total glutathione. (**A**) G6PD activity limits metabolic fluxes through the PPP, which generates pentose phosphate compounds. Generation of these compounds was greater in cells expressing the WT allele of ATM. (**B**) Amount of light (M + 0) and heavy (M + 2) pentose phosphate isobars 6 and 24 hours after cells were labeled with heavy glucose in U2OS cells expressing either WT or C2991L-mutant ATM after endogenous ATM knockdown by each of two shRNAs (1 and 2). Plotted is the mean ± SD of biological triplicates. (**C**) Ratio of the G6PD substrate [glucose-6-phosphate (G6P)] and its downstream product 6-phosphogluconate (6PG) were measured and plotted as described in (B). (**D**) Amount of heavy glutathione plotted as described in (B). *P < 0.05 and **P < 0.01 by Student's t tests.

DISCUSSION

In addition to its role in nuclear DNA DSB sensing and repair, ATM has a redox-signaling function that is initiated by ROS-mediated disulfide-linked dimer formation (*2*, *13*). Here, we found that mitochondria are a physiological source of hydrogen peroxide that can elicit this signaling mode. The primarily nuclear localization of ATM in HeLa cells, as well as the requirement for induction of cellular hydrogen peroxide, indicates that the signaling mechanism could be direct oxidation of ATM by mitochondrial hydrogen peroxide that gains access to the cytoplasm and/or nucleus (*40*). This could occur from perinuclear mitochondria, which have been implicated in redox signaling via diffusion of hydrogen peroxide to the nucleus (*41*). Alternatively, redox signaling via hydrogen peroxide can also be facilitated by enzymes that chemically modify specific cysteine residues in target proteins or that regulate disulfide bond formation (*42*). For example, PRDX2 facilitates hydrogen peroxide–mediated disulfide bond formation in the nuclear transcription factor signal transducers and activators of transcription 3 (*38*). However, although PRDX1 and PRDX2 appear not to have a role in dimerization of ATM based on our results, TRX1 is a negative regulator of this process. The involvement of TRX1 might provide a link between mitochondrial hydrogen peroxide in the cytoplasm and ATM dimer formation in the nucleus because it is located in both compartments (*43*). Thus, mitochondrial hydrogen peroxide could result in reduced nuclear accumulation of TRX1 to allow formation of ATM dimers. Alternatively, a negative regulator of TRX1 could enter the nucleus in response to mitochondrial hydrogen peroxide to inhibit nuclear TRX1 and induce ATM dimers. For example, thioredoxin-interacting protein (TXNIP) is a negative regulator of TRX1 (and TRX2) that appears to shuttle among the nucleus, cytoplasm, and mitochondria (*44*, *45*). Thus, altered TXNIP localization dynamics could be involved in regulation of nuclear TRX1 and hence ATM dimerization.

Despite the independence of DNA damage signaling and redox-sensing functions of ATM, the redox-sensing role of ATM does

make teleological sense with its ultimate goal of protecting the genome. That is, we propose that ATM likely senses an increase in mitochondrial ROS as a potential threat to DNA (nuclear and mitochondrial) and enacts preemptive signaling to detoxify ROS and prime pathways needed to repair the genome. ATM regulates the expression or activity of several antioxidant enzymes including superoxide dismutase 1 and 2, catalase, glutathione peroxidase 1 (*46*), and the rate-limiting enzyme in the PPP, G6PD (*18*). Ionizing radiation activates the PPP through ATM-dependent phosphorylation of HSP27, which promotes its binding to and activation of G6PD (*18*). The PPP provides NADPH needed for many antioxidant pathways and produces ribose-5-phosphate for nucleotide synthesis needed for DNA damage repair (*17*). However, our results show that the redox-sensing function of ATM activates the PPP via expression of G6PD instead of by modulating HSP27 phosphorylation. Although the precise mechanism of gene activation was not elucidated, transcription factors that regulate *G6PD* transcription, including Nrf2, SP1, CREB, and SREBP1 (*47*–*50*), could be targets of ATM redox sensing. Likewise, the regulation of histone methylation by ATM (*51*) might activate the G6PD promoter. It is noteworthy that a major downstream consequence of PPP activation and increased cellular NADPH is enhanced regeneration of reduced thioredoxins. Because TRX1 reduces ATM dimers, a negative feedback loop might exist to modulate redox signaling by ATM. Our metabolic tracing experiments confirmed increased glucose flux through the PPP in WT ATM versus the C2991L-mutant ATM cells, and the WT cells also showed less shunting of glucose-derived heavy carbon atoms into glycolysis and the TCA cycle. This places ATM at critical juncture to regulate central carbohydrate metabolism via its ability to sense mitochondrial hydrogen peroxide or other cellular sources of ROS. We also observed increased glutathione synthesis in the C2991L-mutant ATM cells that we speculate is being up-regulated in an attempt to compensate for the lower flux through the PPP and, hence, less NADPH available to recycle reduced glutathione. There are several points where glutathione synthesis might be activated in the C2991L-mutant ATM cells. For example, the rate-limiting enzyme of glutathione synthesis, glutamate cysteine ligase (GCL), is activated by oxidative stress at the transcriptional and posttranslational level (*52*). The expression of the catalytic and modifier subunit of glutathione cysteine ligase (GCLC and GCLM) is under control of the ROS-responsive transcription factor Nrf2 (*52*). In addition, oxidative stress promotes the interaction of GCLC and GCLM, which increases enzyme activity (*52*, *53*).

Mitochondrial dysfunction and oxidative stress are now recognized as features of A-T (*1*, *54*, *55*), the disease caused by loss-of-function mutations in *ATM*. Our results strongly suggest that these phenotypes are linked through the loss of the redox-sensing function of ATM. In the absence of this function, we propose that cells are unable to convey a homeostatic ROS signal from mitochondria to ATM to up-regulate antioxidant defenses, including activation of the PPP through G6PD gene expression. This, in turn, would lead to accumulation of ROS and oxidative damage to mitochondria and other cellular components observed, as well as protein aggregation, as recently shown (*16*). ATM also regulates autophagy, including mitophagy and pexophagy (*16*, *22*, *34*, *35*), loss of which would likely enhance the oxidative stress phenotype in A-T. We propose that the oxidative stress in A-T is precipitated initially by the loss of the mitochondrial hydrogen peroxide signaling function of ATM that normally would have quelled toxic ROS accumulation and prevented cellular oxidative stress. Reducing mitochondrial hydrogen peroxide in mice can reduce cancer lethality and partially rescue immune phenotypes in the mouse model of A-T (*27*). Thus, in the absence of gene therapy for the disease, potential therapeutic strategies might be to target mitochondrial ROS production directly, enhance cellular antioxidant capacity by increasing G6PD activity or PPP flux, or mitigate other downstream consequences resulting from lack of ATM redox signaling.

MATERIALS AND METHODS

Reagents

Menadione, *N*-ethylmaleimide (NEM), rotenone, and antimycin A were from Sigma-Aldrich. Topotecan and MitoTEMPO were from Enzo Life Sciences. MitoSOX and CM-DCFDA were from Invitrogen. MitoPY1 was from Tocris (no. 4428).

Cell culture, siRNA, and shRNA transfection

HeLa cells and primary MEFs (prepared from day 13.5 embryos) from WT and mCAT mice were propagated in Dulbecco's modified Eagle's medium (DMEM) supplemented with 10% fetal bovine serum (FBS). ATM knockdown in HeLa cells was performed by infecting cells with retrovirus encoding shRNA-targeting ATM (shATM; sequence 1, a gift from D. Stern) or a scrambled (SCR) shRNA. TRX1 knockdown in HeLa cells was performed through infecting cells with lentiviruses containing shRNA-targeting TRX1 (5′-CCGGATCAAGCCTTTCTTTC-3′ ATTCCCTCGAGGGAATG-AAAGAAAGGCTTGATTTTTTG) or EGFP as a control (target sequence: 5′-GCAAGCTGACCCTGAAGTTCAT-3′). In both cases, infected cells were selected in puromycin (0.3 μg/ml). PRDX1 and PRDX2 knockdown was performed by transfecting 20 nM siRNA (reference nos. 130748509 and 130748512; Integrated DNA Technologies) with Lipofectamine RNAiMAX transfection reagent for 72 hours.

The U2OS cell system, in which endogenous ATM is knocked down by shRNA and replaced with inducible, vector-borne WT or C2991L alleles, was described previously by Lee *et al.* (*16*). U2OS cells containing control vector (T-REx Flp-in) or expressing WT or C2991L ATM alleles were cultured in DMEM supplemented with 10% FBS containing blasticidin (15 μg/ml; A1113903, Life Technologies) and hygromycin [200 μg/ml; 400052 (50 ml), Life Technologies]. Depletion of endogenous ATM was performed by incubating cells with lentivirus containing shRNA-targeting ATM (sc-29761-SH, Santa Cruz Biotechnology) overnight and selected in medium containing puromycin (1 μg/ml; Invitrogen) for 5 to 7 days. To induce WT or mutant ATM expression, media were supplemented with doxycycline (1 μg/ml; Sigma-Aldrich) for 3 days. About 16 hours before analysis, the culture medium was changed to DMEM with 10% FBS and doxycycline (1 μg/ml), without puromycin, blasticidin, or hygromycin.

Generation of PRDX1 and PRDX2 knockout HeLa cells

PRDX1 and PRDX2 knockout HeLa cells were generated using the CRISPR-Cas9 system. Guide RNA (gRNA) design was based on the CRISPR design tool developed by the Zhang Lab (http://crispr.mit.edu) (table S1). The single gRNA (sgRNA)–encoding sequences targeting PRDX1 or PRDX2 genes were inserted into the Bbs I site of the p2Tol-U6-sgPal1-HygR vector (sgPal1; Addgene plasmid # 71483) (*56*). Briefly, 2×10^6 cells were transfected with sgRNA construct plasmid (1 μg), p2Tol-cbh-Cas9–blasticidin plasmid (1 μg), and p2Tol-transposase plasmid (1 μg) by using Neon Transfection

System (Invitrogen) according to the manufacturer's protocol (the Cas9 and transponsase plasmids were gifts from R. Sherwood). Three days later, cells were treated with hygromycin B (300 μg/ml) and blasticidin S (10 μg/ml) for 3 days, then isolated using a cell sorter (BD FACSAria Special Order 11 color sorter) into 96-well plates, and allowed to expand for 3 weeks. Several clones per transfection were assessed by Western blot analysis and sequencing of DNA fragments covering the sgRNA target region.

Measurements of ROS

To detect mitochondrial superoxide, cells were grown in 12-well plates and incubated with MitoSOX in DMEM + 10% FBS at a final concentration of 2.5 or 5 μM for 30 min at 37°C. Cells were then trypsinized, washed once with phosphate-buffered saline (PBS), and resuspended in PBS + 0.1% FBS before analyzing MitoSOX fluorescence using Stratedigm 13 in the phycoerythrin 580/30 channel. To measure levels of cellular or mitochondrial hydrogen peroxide, cells were stained with 5 μM CM-DCFDA in DMEM + 10% FBS for 30 min or 10 μM MitoPY1 in serum-free DMEM for 50 min, respectively, after which cells were trypsinized, washed, and pelleted. Cell pellets were resuspended in PBS + 0.1% FBS and immediately measured for fluorescence using Stratedigm 13 in the fluorescein isothiocyanate 530/55 channel. For all flow cytometry experiments, FloJo software was used to determine the mean fluorescence intensity for each sample.

Protein extraction and Western blotting

For standard Western blots to detect proteins, cells were lysed with radioimmunoprecipitation assay buffer [50 mM tris-HCl (pH 8.5), 150 mM NaCl, 1.0% NP-40, 0.5% sodium deoxycholate, 0.1% SDS, 1× protease inhibitor (11836170001, Roche), and 1× phosphatase inhibitor (04906837001, Roche)]. Cell lysates were then sonicated in a Bioruptor sonicator (Diagenode) on high power (7 pulses; 10 s on and 10 s off). Samples were pelleted in a microcentrifuge at 14,000 rpm for 10 min, and supernatants (20 μg) were loaded for Western blot.

For nonreducing Western blots to detect ATM or PRDX1 dimerization, protein extraction was performed in two ways, which gave consistent results. For Figs. 1 and 2, cells were plated at least 16 hours before each experiment. After treatment, cells were scraped in PBS, and proteins were precipitated with 10% trichloroacetic acid on ice for 10 min. Protein pellets were collected by centrifugation at 2000*g* for 5 min. To prevent postlysis oxidation of protein thiols, pellets were washed in 100% acetone and then resuspended in SDS buffer containing NEM [100 mM tris-HCl (pH 6.8), 2% SDS, and NEM (5 mg/ml)] for 30 min at 25°C. Samples were then sonicated in a Bioruptor sonicator (Diagenode) on high power (5 pulses; 10 s on and 10 s off). Samples were pelleted in a microcentrifuge at 14,000 rpm for 10 min, and supernatants were analyzed by Western blot. The ATM dimer (~700 kDa) comigrates with the dimeric 660-kDa form of thyroglobulin. An improvement in this method was used in Figs. 3 and 4 and fig. S1. After drug treatment, cells were washed once with PBS, then incubated in 100 mM NEM in PBS for 5 min at 37°C or 10 min on ice, scraped, and pelleted. Cells were resuspended in lysis buffer [100 mM NaCl, 20 mM tris-HCl (pH 7.5), 0.5% NP-40, 5 mM $CaCl_2$, and 1× protease inhibitor (Roche)] and incubated on ice for 10 min. Nuclear DNA was digested with micrococcal nuclease (30 U/ml) for 8 min at 37°C, and the reaction was terminated by adding 5 mM EGTA (pH 8.0). The nuclei were then lysed by adding SDS to 1% and incubating on ice for 10 min. Samples were spun in a microcentrifuge at 14,000 rpm for 10 min at 4°C, and supernatants were analyzed by Western blot. For either protein extraction method, SDS sample buffer without 2-mercaptoethanol (BME) was added to samples, and 20 μg of protein were loaded into each lane of a 6% polyacrylamide gel to resolve ATM dimers and monomers. Transfer was carried out overnight at 4°C at 30 V using transfer buffer without methanol.

Antibodies used were ATM (1:7500; A-1106, Sigma-Aldrich), phospho-ATM (Ser^{1981}, 1:5000; ab81292, Abcam), phospho-CHK2 (Thr^{68}, 1:1000; 2197, Cell Signaling Technology), CHK2 (1:200; sc5278, Santa Cruz Biotechnology), phospho-H2AX (Ser^{139}, 1:1000; 05-636, Millipore), HSP60 (1:20,000; sc1052, Santa Cruz Biotechnology), catalase (1:5000; C-0979, Sigma-Aldrich), calnexin (1:20,000; sc11397, Santa Cruz Biotechnology), TRX1 (1:15,000; ab26320, Abcam), GAPDH (1:10,000; AM4300, Ambion), G6PD (1:1000; 12263, Cell Signaling Technology), phospho-HSP27 (Ser^{78}, 1:1000; 2405, Cell Signaling Technology), histone H3 (1:2000; ab1791, Abcam), PRDX1 (1:2000; sc-7381, Santa Cruz Biotechnology), and PRDX2 (1:500; sc-23967, Santa Cruz Biotechnology; 1:1000; ab109367, Abcam).

Nuclear fractionation

HeLa cells were grown to ~80% confluence on two 15-cm plates, treated with 30 μM menadione for 1 hour, washed with PBS, and pelleted by centrifugation. The cell pellet was resuspended in 1 ml of buffer containing 0.1 M tris-HCl (pH 6.8), NEM (10 mg/ml), and protease inhibitors (Roche). NEM modification proceeded for 5 min at room temperature after which 300 μl of the sample was removed and saved as whole-cell extract. To the remaining 700 μl, Triton X-100 was added to a final concentration of 0.5%, and cells were incubated on ice for 5 min until visually broken and intact nuclei could be seen. Nuclei were pelleted at 720*g* for 5 min, and the supernatant representing the postnuclear extract was saved. Nuclei were washed three times with NEM buffer with 0.5% Triton X-100 and once with NEM buffer without Triton X-100. Nuclei were resuspended in 700 μl of NEM buffer with 1% SDS and lysed for 10 min on ice. The postnuclear fraction was clarified by three sequential centrifugation steps at 720*g* for 5 min, discarding the pellet each time. To whole-cell, nuclei, and postnuclear fractions, Triton X-100 was added to a final concentration of 1%, and SDS was added to a final concentration of 0.5%. Samples were then sonicated in a Bioruptor sonicator (Diagenode) on high power (5 pulses; 30 s on and 30 s off) and clarified by centrifugation at 14,000 rpm at 4°C for 10 min. Equal volumes (25 μl) of the supernatants were loaded per lane on a 6% SDS-PAGE gel.

Salt extraction of chromatin bound proteins

The protocol used was modified from a previously described method (*57*). HeLa cells (2×10^6) were plated in a 10-cm dish ~16 hours before the experiment. After drug treatment, cells were washed once with 5 ml of PBS, scraped in PBS, and pelleted at 350*g* for 5 min at 4°C. To lyse cells, pellets were resuspended in 50 μl of NETN buffer [100 mM NaCl, 20 mM tris-HCl (pH 7.5), 0.5% NP-40, and 2 mM EDTA] for every 5×10^5 cells and incubated for 15 min on ice during which they were vortexed twice. The nuclei were pelleted in a microcentrifuge at 14,000 rpm for 5 min. The supernatant was moved to a new tube and, after another centrifugation at 14,000 rpm for 5 min, was saved as the cytoplasmic/soluble nuclear protein fraction. The pellet was washed once with 50 μl of NETN buffer, resuspended in 50 μl of nuclear digestion buffer [20 mM tris-HCl (pH 7.5), 150 mM NaCl, 5 mM $CaCl_2$, and micrococcal nuclease (200 U/ml)],

and incubated for 8 min at 37°C. This pellet was saved as the chromatin fraction. After adding 10 µl of 6× SDS sample buffer with BME, the samples were boiled for 5 min and clarified in a microcentrifuge at 13,000 rpm for 10 min at room temperature, and 15 µl of the sample was loaded for SDS-PAGE and Western blot.

Quantitative reverse transcription PCR

RNA was isolated with TRIzol reagent (15596-026, Life Technologies) and converted to complementary DNA (cDNA) using the High-Capacity cDNA Reverse Transcription Kit (Agilent) according to the manufacturer's instructions. cDNA was diluted 1:50, and each 10 µl of reaction contained 4.5 µl of diluted cDNA, 0.5 µl of primer mix (from a 10 µM stock), and 5 µl of Applied Biosystems Fast SYBR Green Master Mix (Life Technologies). PCR was performed on a Bio-Rad CFX96 Real-Time PCR machine in 96-well plates using fast ramp speed. Data were analyzed according to the $\Delta\Delta C_t$ method using GAPDH as a reference gene. Primers used were as following: G6PD, 5′-ACCGCATCGACCACTACCT-3′ (forward) and 5′-TGGGGCCGAAGATCCTGTT-3′ (reverse); GAPDH, 5′-ACAACTTTGGTATCGTGGAAGG-3′ (forward) and 5′-GCCATCACGCCACAGTTTC-3′ (reverse).

G6PD activity assay

The protocol used was modified from a previously described method (*58*). U2OS cells were plated at 1.5×10^6 cells per 10-cm dish ~16 hours before the experiment. Cells were washed with 5 ml of PBS, scraped in 1 ml of PBS, and pelleted. Cell pellets were lysed with 75 µl of NP-40 buffer [100 mM NaCl, 20 mM tris-HCl (pH 7.5), 0.5% NP-40, and 1× protease inhibitor] and incubated for 10 min on ice. Cell lysate was clarified in a microcentrifuge at 14,000 rpm for 10 min at 4°C. The supernatant was diluted to protein (1 µg/µl). In a 96-well plate with black sides and clear bottom, 20 µl of cell lysate and 180 µl of reaction mix [50 mM tris-HCl (pH 8), 1 mM $MgCl_2$, 200 µM glucose-6-phosphate (G7879, Sigma-Aldrich), and 100 µM $NADP^+$ (N0505, Sigma-Aldrich)] were added to each well. To measure NADPH production, fluorescence was measured immediately using excitation at 340 nm and emission at 460 nm on a plate reader (measured at 1-min intervals for 10 min). The fluorescence intensity was plotted versus time, and the slope was calculated. Data points plotted in Fig. 5C are the averaged slope of four technical replicates.

Metabolomics analysis

Metabolomic analyses and tracing experiments with $^{13}C_{1,2,3}$-glucose were performed as previously reported (*59*, *60*). All metabolite standard reagents were purchased from Sigma-Aldrich or Cambridge Isotope Laboratories Inc., unless otherwise stated. U2OS cells in which endogenous ATM was replaced by WT or C2991L alleles of ATM (see details above) were cultured in DMEM without glucose and supplemented with 25 mM $^{13}C_{1,2,3}$-glucose (no. CLM-4673-PK, Cambridge Isotope Laboratories Inc.). Longitudinal sampling of cells and supernatants was performed at 0, 1, 6, and 24 hours from incubation with stable heavy isotope-labeled glucose. Cells (1 million) and supernatants (20 µl) were extracted in 1 ml of ice-cold lysis/extraction buffer (methanol/acetonitrile/water, 5:3:2; triplicate experiment). Samples were then agitated at 4°C for 30 min, followed by centrifugation at 10,000*g* for 15 min at 4°C. Protein pellets were discarded, whereas supernatants were stored at −80°C before metabolomic analyses. Extracts (10 µl) were injected into an ultra-high performance liquid chromatography system (Ultimate 3000, Thermo Fisher Scientific) and run on a Kinetex XB-C18 column (inner diameter, 150 × 2.1 mm; particle size, 1.7 µm; Phenomenex), as previously reported (*59*). Technical mixes were generated by pooling 10 µl of all the cells and supernatants separately. Pooled reference samples were run every 10 analytical runs to control for technical variability, determined as coefficients of variation (CVs). CVs were determined by calculating the ratios of SDs divided by mean measurements for compounds of interest (for example, all isotopologues of lactate) across all technical mix runs. The Q Exactive mass spectrometer (Thermo Fisher Scientific) was operated in full mass spectrometer mode (two microscans) at 70,000 resolution in the 60 to 900 mass/charge ratio range, 4-kV spray voltage, 15 sheath gas, and 5 auxiliary gas, either in negative or positive ion mode. Metabolite assignments and isotopologue distributions were determined using the software Maven (Princeton) (*61*), and assignments were confirmed against 700 standards (IROATech, Sigma-Aldrich).

Glutathione measurements

Total glutathione and GSH/GSSG ratio were measured using the GSH/GSSG-Glo Assay Kit (V6611, Promega) according to the manufacturer's instructions.

Statistical analysis

Unless indicated otherwise, statistical significance was calculated using Student's *t* test, with $^*P < 0.05$ and $^{**}P < 0.01$. Error bars represent the SD.

SUPPLEMENTARY MATERIALS

www.sciencesignaling.org/cgi/content/full/11/538/eaaq0702/DC1

Fig. S1. DCFDA staining of TRX1 knockdown cells and ATM dimerization in *PRDX1* and *PRDX2* knockout cells.

Fig. S2. Additional characterization of the ATM U2OS cell system and replicate experiments with a second ATM shRNA.

Fig. S3. ATM C2991L-mutant cells consume more glucose for glycolysis.

Fig. S4. ATM C2991L-mutant cells flux more carbon from glucose to the TCA cycle.

Fig. S5. ATM C2991L-mutant cells have more total glutathione than WT cells, but GSH/GSSG ratios are similar.

Table S1. Sequences of sgRNAs used to knockout *PRXD1* or *PRDX2* in HeLa cells.

REFERENCES AND NOTES

1. Y. Shiloh, Y. Ziv, The ATM protein kinase: Regulating the cellular response to genotoxic stress, and more. *Nat. Rev. Mol. Cell Biol.* **14**, 197–210 (2013).
2. T. T. Paull, Mechanisms of ATM activation. *Annu. Rev. Biochem.* **84**, 711–738 (2015).
3. S. Matsuoka, B. A. Ballif, A. Smogorzewska, E. R. McDonald III, K. E. Hurov, J. Luo, C. E. Bakalarski, Z. Zhao, N. Solimini, Y. Lerenthal, Y. Shiloh, S. P. Gygi, S. J. Elledge, ATM and ATR substrate analysis reveals extensive protein networks responsive to DNA damage. *Science* **316**, 1160–1166 (2007).
4. C. J. Bakkenist, M. B. Kastan, DNA damage activates ATM through intermolecular autophosphorylation and dimer dissociation. *Nature* **421**, 499–506 (2003).
5. S. Ditch, T. T. Paull, The ATM protein kinase and cellular redox signaling: Beyond the DNA damage response. *Trends Biochem. Sci.* **37**, 15–22 (2012).
6. A. Barzilai, G. Rotman, Y. Shiloh, ATM deficiency and oxidative stress: A new dimension of defective response to DNA damage. *DNA Repair* **1**, 3–25 (2002).
7. C. Barlow, P. A. Dennery, M. K. Shigenaga, M. A. Smith, J. D. Morrow, L. J. Roberts II, A. Wynshaw-Boris, R. L. Levine, Loss of the ataxia–telangiectasia gene product causes oxidative damage in target organs. *Proc. Natl. Acad. Sci. U.S.A.* **96**, 9915–9919 (1999).
8. J. Kim, P. K. Y. Wong, Loss of ATM impairs proliferation of neural stem cells through oxidative stress-mediated p38 MAPK signaling. *Stem Cells* **27**, 1987–1998 (2009).
9. J. Kim, P. K. Y. Wong, Oxidative stress is linked to ERK1/2-p16 signaling-mediated growth defect in ATM-deficient astrocytes. *J. Biol. Chem.* **284**, 14396–14404 (2009).
10. K. Ito, A. Hirao, F. Arai, K. Takubo, S. Matsuoka, K. Miyamoto, M. Ohmura, K. Naka, K. Hosokawa, Y. Ikeda, T. Suda, Reactive oxygen species act through p38 MAPK to limit the lifespan of hematopoietic stem cells. *Nat. Med.* **12**, 446–451 (2006).
11. J. Bagley, G. Singh, J. Iacomini, Regulation of oxidative stress responses by ataxia-telangiectasia mutated is required for T cell proliferation. *J. Immunol.* **178**, 4757–4763 (2007).

12. K. Ito, K. Takubo, F. Arai, H. Satoh, S. Matsuoka, M. Ohmura, K. Naka, M. Azuma, K. Miyamoto, K. Hosokawa, Y. Ikeda, T. W. Mak, T. Suda, A. Hirao, Regulation of reactive oxygen species by *Atm* is essential for proper response to DNA double-strand breaks in lymphocytes. *J. Immunol.* **178**, 103–110 (2007).
13. Z. Guo, S. Kozlov, M. F. Lavin, M. D. Person, T. T. Paull, ATM activation by oxidative stress. *Science* **330**, 517–521 (2010).
14. E. A. Schroeder, N. Raimundo, G. S. Shadel, Epigenetic silencing mediates mitochondria stress-induced longevity. *Cell Metab.* **17**, 954–964 (2013).
15. Z. Guo, R. Deshpande, T. T. Paull, ATM activation in the presence of oxidative stress. *Cell Cycle* **9**, 4805–4811 (2010).
16. J.-H. Lee, M. R. Mand, C.-H. Kao, Y. Zhou, S. W. Ryu, A. L. Richards, J. J. Coon, T. T. Paull, ATM directs DNA damage responses and proteostasis via genetically separable pathways. *Sci. Signal.* **11**, eaan5598 (2018).
17. K. C. Patra, N. Hay, The pentose phosphate pathway and cancer. *Trends Biochem. Sci.* **39**, 347–354 (2014).
18. C. Cosentino, D. Grieco, V. Costanzo, ATM activates the pentose phosphate pathway promoting anti-oxidant defence and DNA repair. *EMBO J.* **30**, 546–555 (2011).
19. M. D. Brand, The sites and topology of mitochondrial superoxide production. *Exp. Gerontol.* **45**, 466–472 (2010).
20. M. Ambrose, J. V. Goldstine, R. A. Gatti, Intrinsic mitochondrial dysfunction in ATM-deficient lymphoblastoid cells. *Hum. Mol. Genet.* **16**, 2154–2164 (2007).
21. J. S. Eaton, Z. P. Lin, A. C. Sartorelli, N. D. Bonawitz, G. S. Shadel, Ataxia-telangiectasia mutated kinase regulates ribonucleotide reductase and mitochondrial homeostasis. *J. Clin. Invest.* **117**, 2723–2734 (2007).
22. Y. A. Valentin-Vega, K. H. Maclean, J. Tait-Mulder, S. Milasta, M. Steeves, F. C. Dorsey, J. L. Cleveland, D. R. Green, M. B. Kastan, Mitochondrial dysfunction in ataxia-telangiectasia. *Blood* **119**, 1490–1500 (2012).
23. X. Fu, S. Wan, Y. L. Lyu, L. F. Liu, H. Qi, Etoposide induces ATM-dependent mitochondrial biogenesis through AMPK activation. *PLOS ONE* **3**, e2009 (2008).
24. K. Ito, A. Hirao, F. Arai, S. Matsuoka, K. Takubo, I. Hamaguchi, K. Nomiyama, K. Hosokawa, K. Sakurada, N. Nakagata, Y. Ikeda, T. W. Mak, T. Suda, Regulation of oxidative stress by ATM is required for self-renewal of haematopoietic stem cells. *Nature* **431**, 997–1002 (2004).
25. R. Schubert, L. Erker, C. Barlow, H. Yakushiji, D. Larson, A. Russo, J. B. Mitchell, A. Wynshaw-Boris, Cancer chemoprevention by the antioxidant tempol in *Atm*-deficient mice. *Hum. Mol. Genet.* **13**, 1793–1802 (2004).
26. R. Reliene, E. Fischer, R. H. Schiestl, Effect of *N*-acetyl cysteine on oxidative DNA damage and the frequency of DNA deletions in *Atm*-deficient mice. *Cancer Res.* **64**, 5148–5153 (2004).
27. A. D. D'Souza, I. A. Parish, D. S. Krause, S. M. Kaech, G. S. Shadel, Reducing mitochondrial ROS improves disease-related pathology in a mouse model of ataxia-telangiectasia. *Mol. Ther.* **21**, 42–48 (2013).
28. Y. Pan, G. S. Shadel, Extension of chronological life span by reduced TOR signaling requires down-regulation of Sch9p and involves increased mitochondrial OXPHOS complex density. *Aging* **1**, 131–145 (2009).
29. L. A. Sena, N. S. Chandel, Physiological roles of mitochondrial reactive oxygen species. *Mol. Cell* **48**, 158–167 (2012).
30. G. S. Shadel, T. L. Horvath, Mitochondrial ROS signaling in organismal homeostasis. *Cell* **163**, 560–569 (2015).
31. B. C. Dickinson, V. S. Lin, C. J. Chang, Preparation and use of MitoPY1 for imaging hydrogen peroxide in mitochondria of live cells. *Nat. Protoc.* **8**, 1249–1259 (2013).
32. K. W. Lee, D. J. Lee, J. Y. Lee, D. H. Kang, J. Kwon, S. W. Kang, Peroxiredoxin II restrains DNA damage-induced death in cancer cells by positively regulating JNK-dependent DNA repair. *J. Biol. Chem.* **286**, 8394–8404 (2011).
33. X. Wang, S. He, J.-M. Sun, G. P. Delcuve, J. R. Davie, Selective association of peroxiredoxin 1 with genomic DNA and *COX-2* upstream promoter elements in estrogen receptor negative breast cancer cells. *Mol. Biol. Cell* **21**, 2987–2995 (2010).
34. A. Alexander, S.-L. Cai, J. Kim, A. Nanez, M. Sahin, K. H. MacLean, K. Inoki, K.-L. Guan, J. Shen, M. D. Person, D. Kusewitt, G. B. Mills, M. B. Kastan, C. L. Walker, ATM signals to TSC2 in the cytoplasm to regulate mTORC1 in response to ROS. *Proc. Natl. Acad. Sci. U.S.A.* **107**, 4153–4158 (2010).
35. J. Zhang, D. N. Tripathi, J. Jing, A. Alexander, J. Kim, R. T. Powell, R. Dere, J. Tait-Mulder, J.-H. Lee, T. T. Paull, R. K. Pandita, V. K. Charaka, T. K. Pandita, M. B. Kastan, C. L. Walker, ATM functions at the peroxisome to induce pexophagy in response to ROS. *Nat. Cell Biol.* **17**, 1259–1269 (2015).
36. D. Watters, P. Kedar, K. Spring, J. Bjorkman, P. Chen, M. Gatei, G. Birrell, B. Garrone, P. Srinivasa, D. I. Crane, M. F. Lavin, Localization of a portion of extranuclear ATM to peroxisomes. *J. Biol. Chem.* **274**, 34277–34282 (1999).
37. W. H. Watson, D. P. Jones, Oxidation of nuclear thioredoxin during oxidative stress. *FEBS Lett.* **543**, 144–147 (2003).
38. M. C. Sobotta, W. Liou, S. Stöcker, D. Talwar, M. Oehler, T. Ruppert, A. N. D. Scharf, T. P. Dick, Peroxiredoxin-2 and STAT3 form a redox relay for H_2O_2 signaling. *Nat. Chem. Biol.* **11**, 64–70 (2015).
39. R. M. Jarvis, S. M. Hughes, E. C. Ledgerwood, Peroxiredoxin 1 functions as a signal peroxidase to receive, transduce, and transmit peroxide signals in mammalian cells. *Free Radic. Biol. Med.* **53**, 1522–1530 (2012).
40. M. P. Murphy, Modulating mitochondrial intracellular location as a redox signal. *Sci. Signal.* **5**, pe39 (2012).
41. A. B. Al-Mehdi, V. M. Pastukh, B. M. Swiger, D. J. Reed, M. R. Patel, G. C. Bardwell, V. V. Pastukh, M. F. Alexeyev, M. N. Gillespie, Perinuclear mitochondrial clustering creates an oxidant-rich nuclear domain required for hypoxia-induced transcription. *Sci. Signal.* **5**, ra47 (2012).
42. C. R. Reczek, N. S. Chandel, ROS-dependent signal transduction. *Curr. Opin. Cell Biol.* **33**, 8–13 (2015).
43. Y.-M. Go, D. P. Jones, Redox compartmentalization in eukaryotic cells. *Biochim. Biophys. Acta* **1780**, 1273–1290 (2008).
44. G. Saxena, J. Chen, A. Shalev, Intracellular shuttling and mitochondrial function of thioredoxin-interacting protein. *J. Biol. Chem.* **285**, 3997–4005 (2010).
45. C. World, O. N. Spindel, B. C. Berk, Thioredoxin-interacting protein mediates TRX1 translocation to the plasma membrane in response to tumor necrosis factor-α: A key mechanism for vascular endothelial growth factor receptor-2 transactivation by reactive oxygen species. *Arterioscler. Thromb. Vasc. Biol.* **31**, 1890–1897 (2011).
46. S. Yalcin, X. Zhang, J. P. Luciano, S. K. Mungamuri, D. Marinkovic, C. Vercherat, A. Sarkar, M. Grisotto, R. Taneja, S. Ghaffari, Foxo3 is essential for the regulation of ataxia telangiectasia mutated and oxidative stress-mediated homeostasis of hematopoietic stem cells. *J. Biol. Chem.* **283**, 25692–25705 (2008).
47. B. Liu, M. Fang, Z. He, D. Cui, S. Jia, X. Lin, X. Xu, T. Zhou, W. Liu, Hepatitis B virus stimulates G6PD expression through HBx-mediated Nrf2 activation. *Cell Death Dis.* **6**, e1980 (2015).
48. J. A. Leopold, A. Dam, B. A. Maron, A. W. Scribner, R. Liao, D. E. Handy, R. C. Stanton, B. Pitt, J. Loscalzo, Aldosterone impairs vascular reactivity by decreasing glucose-6-phosphate dehydrogenase activity. *Nat. Med.* **13**, 189–197 (2007).
49. K. Duvel, J. L. Yecies, S. Menon, P. Raman, A. I. Lipovsky, A. L. Souza, E. Triantafellow, Q. Ma, R. Gorski, S. Cleaver, M. G. Vander Heiden, J. P. MacKeigan, P. M. Finan, C. B. Clish, L. O. Murphy, B. D. Manning, Activation of a metabolic gene regulatory network downstream of mTOR complex 1. *Mol. Cell* **39**, 171–183 (2010).
50. K. Makarona, V. S. Caputo, J. R. Costa, B. Liu, D. O'Connor, D. Iskander, D. Roper, L. Robertson, N. Bhatnagar, E. Terpos, E. Georgiou, M. Papaioannou, D. M. Layton, L. Luzzatto, I. Roberts, A. Karadimitris, Transcriptional and epigenetic basis for restoration of G6PD enzymatic activity in human G6PD-deficient cells. *Blood* **124**, 134–141 (2014).
51. M. K. Ayrapetov, O. Gursoy-Yuzugullu, C. Xu, Y. Xu, B. D. Price, DNA double-strand breaks promote methylation of histone H3 on lysine 9 and transient formation of repressive chromatin. *Proc. Natl. Acad. Sci. U.S.A.* **111**, 9169–9174 (2014).
52. S. C. Lu, Glutathione synthesis. *Biochim. Biophys. Acta* **1830**, 3143–3153 (2013).
53. C. M. Krejsa, C. C. Franklin, C. C. White, J. A. Ledbetter, G. L. Schieven, T. J. Kavanagh, Rapid activation of glutamate cysteine ligase following oxidative stress. *J. Biol. Chem.* **285**, 16116–16124 (2010).
54. A. Guleria, S. Chandna, ATM kinase: Much more than a DNA damage responsive protein. *DNA Repair* **39**, 1–20 (2016).
55. G. S. Shadel, Expression and maintenance of mitochondrial DNA: New insights into human disease pathology. *Am. J. Pathol.* **172**, 1445–1456 (2008).
56. M. Arbab, S. Srinivasan, T. Hashimoto, N. Geijsen, R. I. Sherwood, Cloning-free CRISPR. *Stem Cell Rep.* **5**, 908–917 (2015).
57. C. Bian, Q. Chen, X. Yu, The zinc finger proteins ZNF644 and WIZ regulate the G9a/GLP complex for gene repression. *Elife* **4**, e05606 (2015).
58. W.-N. Tian, L. D. Braunstein, J. Pang, K. M. Stuhlmeier, Q.-C. Xi, X. Tian, R. C. Stanton, Importance of glucose-6-phosphate dehydrogenase activity for cell growth. *J. Biol. Chem.* **273**, 10609–10617 (1998).
59. A. D'Alessandro, T. Nemkov, T. Yoshida, A. Bordbar, B. O. Palsson, K. C. Hansen, Citrate metabolism in red blood cells stored in additive solution-3. *Transfusion* **57**, 325–336 (2017).
60. J. A. Reisz, M. J. Wither, M. Dzieciatkowska, T. Nemkov, A. Issaian, T. Yoshida, A. J. Dunham, R. C. Hill, K. C. Hansen, A. D'Alessandro, Oxidative modifications of glyceraldehyde 3-phosphate dehydrogenase regulate metabolic reprogramming of stored red blood cells. *Blood* **128**, e32–e42 (2016).
61. M. F. Clasquin, E. Melamud, J. D. Rabinowitz, LC-MS data processing with MAVEN: A metabolomic analysis and visualization engine. *Curr. Protoc. Bioinformatics* **37**, 14.11.1–14.11.23 (2012).

Acknowledgments: We wish to thank L. Newman for help troubleshooting the use of redox-sensitive dyes, D. Stern for providing the human ATM shRNA, and S. McKay for helpful advise throughout the project. **Funding:** This work was supported by NIH R01 AG047632 and

R33 ES025636, a grant from the A-T Children's Project, the Audrey Geisel Chair Fund, the Joseph A. and Lucille K. Chair fund to G.S.S., and NIH R01 GM065204 to V.N.G. B.E.C. was supported by NIH NRSA NS077723, E.A.S. by NIH F31AG043242, Y.Z. by the China Scholarship Counsel, and A.D. by the Webb-Waring Early Career Award from the Boettcher Foundation.
Author contributions: Y.Z. performed experiments and wrote the manuscript. J.-H.L. provided critical reagents and data analysis. T.T.P. provided critical reagents, data analysis, and funding. S.G. performed experiments and data analysis. A.D. performed the data analysis, wrote the manuscript, and provided the funding. Q.D. provided critical reagents. V.N.G. provided critical reagents and funding. E.A.S. and S.K.S. performed experiments. B.E.C. performed experiments, wrote the manuscript, and provided the funding. G.S.S. wrote the manuscript, performed the data analysis, and provided the funding. **Competing interests:** The authors declare that they have no competing interests. **Data and materials availability:** Transfer of reagents used in this work may require a material transfer agreement. All data needed to evaluate the conclusions in the paper are present in the paper and/or the Supplementary Materials.

Submitted 27 September 2017
Accepted 19 June 2018
Published 10 July 2018
10.1126/scisignal.aaq0702

Citation: Y. Zhang, J.-H. Lee, T. T. Paull, S. Gehrke, A. D'Alessandro, Q. Dou, V. N. Gladyshev, E. A. Schroeder, S. K. Steyl, B. E. Christian, G. S. Shadel, Mitochondrial redox sensing by the kinase ATM maintains cellular antioxidant capacity. *Sci. Signal.* **11**, eaaq0702 (2018).

Science Signaling

Mitochondrial redox sensing by the kinase ATM maintains cellular antioxidant capacity

Yichong Zhang, Ji-Hoon Lee, Tanya T. Paull, Sarah Gehrke, Angelo D'Alessandro, Qianhui Dou, Vadim N. Gladyshev, Elizabeth A. Schroeder, Samantha K. Steyl, Brooke E. Christian and Gerald S. Shadel

Sci. Signal. **11** (538), eaaq0702.
DOI: 10.1126/scisignal.aaq0702

Antioxidant role of ATM

The kinase ATM is integral to repairing damaged DNA. Hence, its loss has severe consequences for the development of disease. However, ATM also separately functions in the response to reactive oxygen species (ROS). ROS cause oxidative stress, a classic feature of cells in patients with the neurodegenerative disease ataxia telangiectasia (A-T), for which ATM was named. Using a mutant that impairs only the ROS-responsive function of ATM, Zhang *et al*. found that ROS produced by the mitochondria trigger the dimerization of ATM, which indirectly increased the expression and activity of an enzyme that shifts glucose flux from glycolysis and lactic acid production to the pentose phosphate pathway (PPP) and NADPH production, thereby increasing the antioxidant capacity of cells. These findings show how loss of the ROS-sensing, antioxidant function of ATM may contribute to the phenotypes of A-T.